Solar Energy Materials & Solar Cells 220 (2021) 110850

Contents lists available at ScienceDirect

Solar Energy Materials and Solar Cells

journal homepage: http://www.elsevier.com/locate/solmat

Significant solar energy absorption of MXene $Ti_3C_2T_x$ nanofluids via localized surface plasmon resonance

Debing Wang [a,1], Yuxin Fang [b,1], Wei Yu [a,*], Lingling Wang [a,c], Huaqing Xie [a], Yanan Yue [b,d,**]

[a] College of Engineering, Shanghai Key Laboratory of Engineering Materials Application and Evaluation, Shanghai Polytechnic University, Shanghai, 201209, China
[b] Key Laboratory of Hydraulic Machinery Transients (MOE), School of Power and Mechanical Engineering, Wuhan University, Wuhan, Hubei, 430072, China
[c] Research Center of Resource Recycling Science and Engineering, Shanghai Polytechnic University, Shanghai, 201209, China
[d] Department of Mechanical and Manufacturing Engineering, Miami University, Oxford, OH, 45056, United States

ARTICLE INFO

Keywords:
Solar energy
MXene $Ti_3C_2T_x$
Nanofluids
Photothermal
Localized surface plasmon resonance

ABSTRACT

Efficiency is an important factor in the utilization of solar energy. Direct absorption solar energy collectors (DASCs), a new generation collector of converting solar irradiation into heat directly by nanofluids, is regarded as a promising solution for capturing solar energy with high efficiency. Both good stability and high absorption ability are crucial for nanofluids to be an ideal working fluid of DASCs. In this work, we synthesize hyperstable $Ti_3C_2T_x$-H_2O nanofluids as the working fluids of DASCs and investigate its photothermal conversion performance. The results show that the maximum conversion efficiency of thin-layer $Ti_3C_2T_x$ nanofluids achieves 91.9% at a very low mass fraction of 0.02 wt%, which is higher than that of multi-layer $Ti_3C_2T_x$ samples. Based on the experimental results, a simulation model is built to observe the radiation energy transformation in DASCs and results show that better photothermal performance of thin-layer MXene $Ti_3C_2T_x$ stems from its stronger localized surface plasmon resonance (LSPR) effect. Besides, the coupling effect and the shape of $Ti_3C_2T_x$ particles also play important roles in photothermal absorption and conversion. Based on our experimental and numerical results, the $Ti_3C_2T_x$-H_2O nanofluids have great potential in solar energy harvesting.

1. Introduction

In recent years, much attention has been focused on solar energy applications, among them, the conversion of solar energy to thermal energy is the most potential and simplest way [1,2]. The key factor affecting its photothermal efficiency is the selection of collector and working fluids. Direct absorption solar energy collectors (DASCs), a new generation collector of converting solar irradiation into heat directly by working fluids, have been intensively studied [3,4]. Compared with the traditional collectors, this approach is simpler and more efficient by removing the light absorption coating to reduce the heat loss to surroundings [5,6]. It is desirable to find a kind of working fluid which has both excellent photo-absorption ability and high thermal conductivity in DASCs. The absorption of the traditional pure working fluids is weak, and current knowledge shows that the absorption efficiency and heat transfer of fluids can be greatly enhanced with the addition of nanoparticles (named nanofluids) [7,8]. Under the incident sunlight, the temperature of nanofluids can be dramatically increased due to the additional light absorption of nanoparticles. The energy absorbed by nanoparticles will be dispersed in the base fluids through convection and conduction, thus, the overall heat collection efficiency can be improved [9].

Various nanofluids containing carbon nanomaterials [10,11], metals nanoparticles [12,13] and other metal oxides [14,15] have been used for working fluid. However, most of them are insoluble in base fluid such as water and oil, which inevitably results in aggregation due to the poor dispersibility [16]. Although chemical modification offers a feasible approach to improve dispersibility, the performance of their photothermal efficiency and thermal conductivity will be adversely affected

* Corresponding author.
** Corresponding author. Key Laboratory of Hydraulic Machinery Transients (MOE), School of Power and Mechanical Engineering, Wuhan University, Wuhan, Hubei, 430072, China.
E-mail addresses: yuwei@sspu.edu.cn (W. Yu), yyue@miamioh.edu (Y. Yue).
[1] Both authors contributed equally to this work and should be considered co-first authors.

https://doi.org/10.1016/j.solmat.2020.110850
Received 2 July 2020; Received in revised form 12 October 2020; Accepted 19 October 2020
Available online 2 November 2020

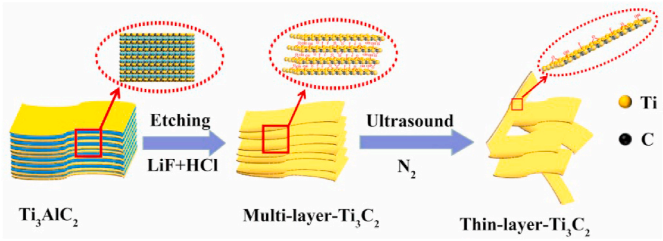

Fig. 1. Preparation process of multi-layer $Ti_3C_2T_x$ and thin-layer $Ti_3C_2T_x$.

due to the existence of surfactants [17]. Recently, the nanofluids containing plasmonic nanoparticles have attracted enormous attention owing to nanoparticles' localized surface plasmon resonance (LSPR) effect, in which the surface conductive electrons collectively resonate in the irradiation of incident light, exhibiting a strong absorption characteristic peaks in the spectrum [18]. Both near electric-field properties and far-field absorption properties are strongly enhanced at the resonance frequency [19]. Pallavicini et al. proved that bulk materials coated with monolayers of gold nanostars have high photothermal conversion efficiency due to the LSPR effect that can be changed through the coating of monolayer [20]. Wang et al. investigated the photothermal conversion performance of near-spherical gold nanofluids with strong LSPR and found that the Au/H_2O can achieve high temperature rise [21].

MXene, a new 2D graphene analogues consisted of early transition metal carbides or carbonitrides, was first introduced in 2011 and rapidly found its applications in energy storage [22,23], electromagnetic interference shielding [24] and supercapacitors [25], *etc*. Among them, $Ti_3C_2T_x$, as the most typical representative of MXene, has already shown great promise in the application of solar energy system due to its high electrical conductivity and extraordinary absorb light ability [26]. Shahzad et al. found that flexible $Ti_3C_2T_x$ films with thickness ranging from 1 to 45 μm exhibit excellent electric conductivities and EMI (electromagnetic interference) shielding capabilities [27]. Shi et al. revealed the high photothermal-conversion efficiency of Ti_3C_2 nanosheets in vitro/in vivo photothermal ablation of tumor [28]. Yahya et al. dispersed the MXene into palm oil and determined its dynamic viscosity [29]. Wang et al. prepared a self-floating MXene membrane for solar steam generation and discovered that the internal light-to-heat conversion efficiency approaches 100% [30]. More importantly, it also found that MXene $Ti_3C_2T_x$ exhibits a strong LSPR effect of semimetal character in the near-infrared (NIR) window (808 nm) and excellent water-solubility [28]. These attributes put the nanofluids containing MXene $Ti_3C_2T_x$ on the way to be a promising working fluid. Aslfattahi also found that the performance of concentrated photovoltaic thermal collector can be improved by using MXene based silicone oil nanofluids as working fluids [31]. However, there is little research reveals the MXene $Ti_3C_2T_x$ photothermal conversion performance in DASCs, in particular observation of the optical absorption property in the micro-nano scale.

In this work, the hyperstable $Ti_3C_2T_x$-H_2O nanofluids are prepared by two step method firstly. The photothermal conversion performance with the different concentration nanofluids containing multi-layer $Ti_3C_2T_x$ and thin-layer $Ti_3C_2T_x$ are thoroughly studied, which is also compared with other nanofluids including graphene, graphitic carbon (ZNG) and ZrC. Based on the experimental results, a simulation model is built to observe the Radiation energy transformation of MXene $Ti_3C_2T_x$ in DASCs. In particular, the coupling effects of surface plasmons on photo-absorption are discussed in detail. This research broadens the application of MXene ($Ti_3C_2T_x$) in the field of solar thermal utilization and breaks the limitation of fluid instability on DASCs.

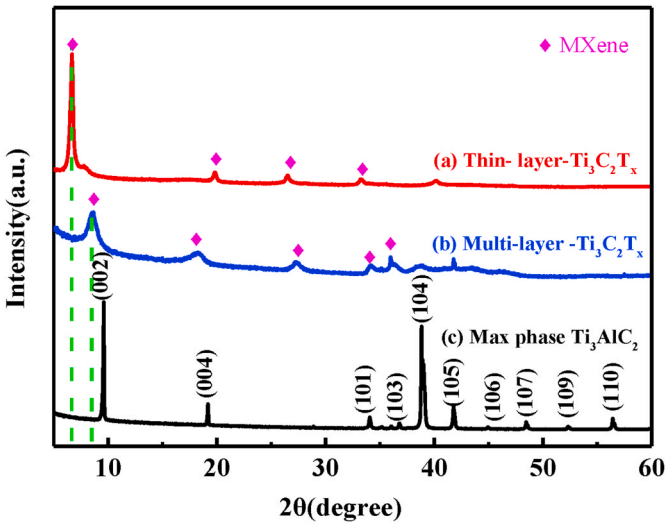

Fig. 2. XRD patterns of Max phase Ti_3AlC_2; multi-layer $Ti_3C_2T_x$ and thin-layer $Ti_3C_2T_x$.

2. Sample preparations and experimental details

2.1. Synthesis of $Ti_3C_2T_x$ nanofluids

The crude material Ti_3AlC_2 MAX (400 mesh) in this study is purchased from 11 Technology Co., Ltd. The other chemicals including LiF and HCl are available from Sinopharm Chemical Reagent Co. Ltd., Shanghai and directly used without further purification. $Ti_3C_2T_x$ is prepared by the solvent erosion method as shown in Fig. 1. Typically, 1.6 g of LiF is dissolved in 20 mL 9 M HCl solution, and then slowly added into the Teflon beaker containing 1 g of Ti_3AlC_2 in 45 °C oil bath under stirring. The suspension is stirred for 24 h and then washed and centrifuged with deionized water until the pH value of nearly neutral conditions. The collected $Ti_3C_2T_x$ deposition is divided into two parts: one is dried in the vacuum oven at 45 °C for 12 h and the multi-layer $Ti_3C_2T_x$ is obtained, the other is dispersed in 100 mL deionized water and ultrasonicated 3 h with nitrogen protection. The suspension is centrifuged 30 min at 3500 rpm, and the supernatant is collected to obtain the thin-layer $Ti_3C_2T_x$. The nanofluids containing multi-layer $Ti_3C_2T_x$, thin-layer $Ti_3C_2T_x$ and Ti_3AlC_2 are prepared by sonication in the base liquid for 20 min to be dispersed. Other nanofluids containing Graphene, ZrC and ZNG [32] are obtained by the similar method.

2.2. Characterization of samples

The crystalline structure of samples is performed by an X-ray diffractometer (D8-Advance, Bruker AXS GmbH, Germany) with Cu-Kα radiation from 5° to 60° at a scanning speed of 8°/min. It can be seen from Fig. 2, peaks at 2θ values of 9.6, 19.1, 34.1, 36.7, 38.9, 41.7, 44.9, 48.5, 52.3 and 56.4° are attributed to (002), (004), (101), (103), (104), (105), (106), (107), (109) and (110) planes of Ti_3AlC_2 powders, respectively, indicating the purchased crude material Ti_3AlC_2 powders are phase-pure. After etching by the mixture of LiF and HCl, the characteristic (104) peaks belonging to Ti_3AlC_2 eventually vanish and the (002) peaks of $Ti_3C_2T_x$ shift to a smaller angle. What's more, the shifting becomes more evident owing to the expanded distance of the crystal face of $Ti_3C_2T_x$ after ultrasonic exfoliation. All these analyses indicate that the Al-atoms has been successfully removed from Ti_3AlC_2 and the pure phase of $Ti_3C_2T_x$ is prepared.

The images of scanning electron microscopy (SEM) tell the story of the formation of thin-layer Ti_3C_2 powders, which is measured at an accelerating voltage of 10 kV and the result as shown in Fig. 3a-c. It can be seen from Fig. 3b that the etched $Ti_3C_2T_x$ shows typical accordion-

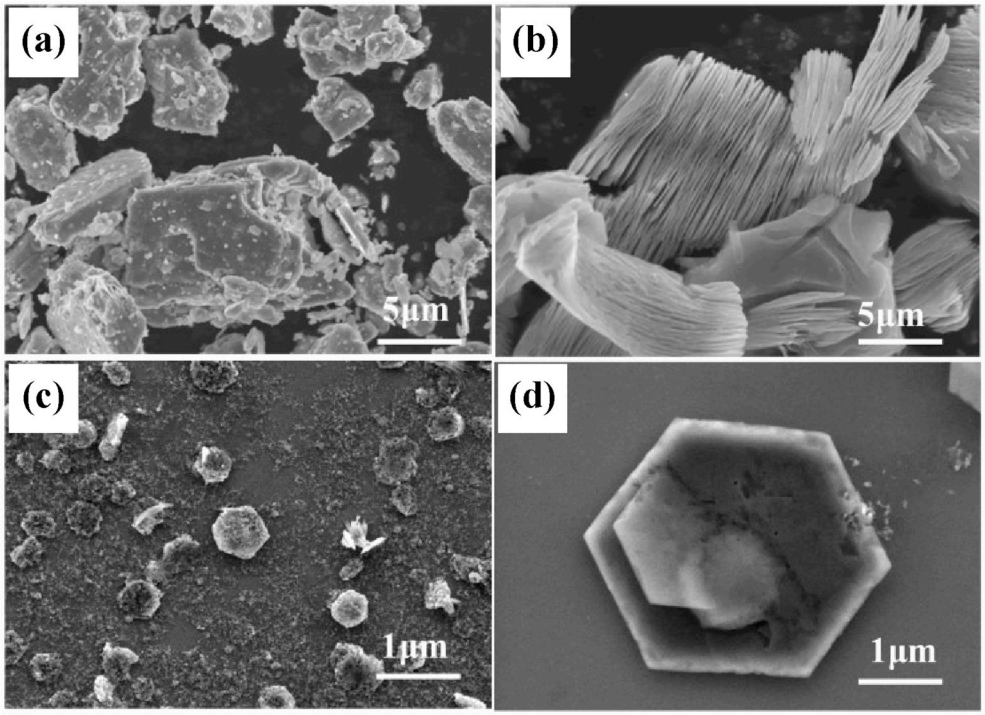

Fig. 3. SEM of a) Max phase Ti_3AlC_2; b) multi-layer $Ti_3C_2T_x$; c) and d) thin-layer $Ti_3C_2T_x$.

like structures with clearly visible open layering, indicating that the Al-atoms has been successfully removed from Ti_3AlC_2, and multi-layer $Ti_3C_2T_x$ is well stacked by uniform sheets (Fig. 1a, b) and its thickness is about 1–2 μm. Thin-layer Ti $_3C_2T_x$ is obtained after further exfoliation by ultrasonic treatment. As Fig. 3c-d show that the fully exfoliated samples have flaky structures.

2.3. Evaluation of the photothermal conversion properties

The solar irradiation absorption of nanofluids is evaluated by a self-assembled photothermal conversion system which has been depicted in our previous paper [33]. In this work, 4 ml of nanofluids are sealed in a 4 cm × 1 cm × 1 cm cuvette inserted into the thermal insulator at room temperature of 25 °C and the top surface area (4 cm × 1 cm) are exposed to 1000 Wm^{-2} irradiation of solar simulator. A thermocouple fixed in the central of nanofluids is used to record the temperature every 5s by a data collector. And each experimental result was repeated 3 times. The solar simulator is turned off after the temperature of nanofluids reaches the equilibrium for a duration of time and then the nanofluids are cooled naturally to room temperature. The photothermal conversion efficiency can be calculated by Formula (1) [34]:

$$\eta = \frac{(t_{eq} - t_{am})c_w m_w B}{AS_m} \tag{1}$$

Where t_{eq} and t_{am} are the equilibrium temperature and room temperature, respectively. m_w and c_p represent the mass and specific heat of nanofluids, respectively. A and S_m are the radiation area (4.0 cm^2) and irradiation power (1000 Wm^{-2}) of solar simulator received by nanofluids. B, the constant rate of heat dissipation, is equal to $Ln[(t_{(t)}\text{-}t_a)/(t_e\text{-}t_a)]$ dt [34].

2.4. Uncertainty analysis in measurements

In this study, the total errors are mainly stemmed from random (precision) which is determined by Formula (2) [35]:

$$u_r^2 = \left(\frac{\partial r}{\partial X1}\right)^2 u_{X1}^2 + \left(\frac{\partial r}{\partial X2}\right)^2 u_{X2}^2 + \cdots + \left(\frac{\partial r}{\partial Xj}\right)^2 u_{Xj}^2 \tag{2}$$

where U_r and U_{Xi} are the total uncertainty and the standard deviation of independent quantities, respectively.∂r∂Xj2uXj2.

The uncertainty of the photothermal conversion efficiency is decided by the mass m_w (± 0.01 g), the specific heat c_w (± 1%), irradiation intensity S_m (± 4%), precision of thermocouples t (±0.2 °C) and the solar incident areas A is determined by d (± 0.01 mm) according to the Eq (1). It can be obtained by the following equation:

$$\frac{U\eta}{\eta} = \left[\left(\frac{Um}{m}\right)^2 + \left(\frac{Ucw}{cw}\right)^2 + \left(\frac{Usm}{sm}\right)^2 + \left(\frac{Ut}{t}\right)^2 + \left(\frac{UA}{A}\right)^2\right]^{0.5}$$

$$\frac{Um}{m} = \frac{0.01}{4} = 0.25\%,\ \frac{Ucw}{cw} \le 1\%,\ \frac{UG}{G} = \frac{0.04}{1000} = 0.004\%,$$

$$\frac{Ut}{t} = \frac{0.2}{25} = 0.8\%,\ \frac{UA}{mA} = \left(2\left(\frac{Ud}{d}\right)^2\right)^{0.5} = \left(2\left(\frac{0.1}{4}\right)^2\right)^{0.5} = 3.5\%$$

The final result is $\frac{U\eta}{\eta} = 3.73\%$.

3. Experimental results and discussion

3.1. Stability of $Ti_3C_2T_x$ nanofluids

The poor stability of nanofluids is one of the bottlenecks to limit application in the solar thermal utilization fields. It has been reported that the characteristic absorption peaks of $Ti_3C_2T_x$ are at wavelength 808 nm in the near-infrared spectrum [36], which also record by UV–Vis–NIR (Cary 5000, USA) at room temperature (Fig. 4a). Therefore, the transmittance testing of nanofluids with the mass fraction of 0.05 wt % at 808 nm is used to characterize the stability at different storage times (2 days, 4 days, 6 days, 8 days, 10 days, 12 days, 14 days). It can be seen from Fig. 4b that the transmittance of nanofluids containing Ti_3AlC_2 and multi-layer $Ti_3C_2T_x$ gradually increase along with the extension of the settling time, suggesting that the nanofluids containing

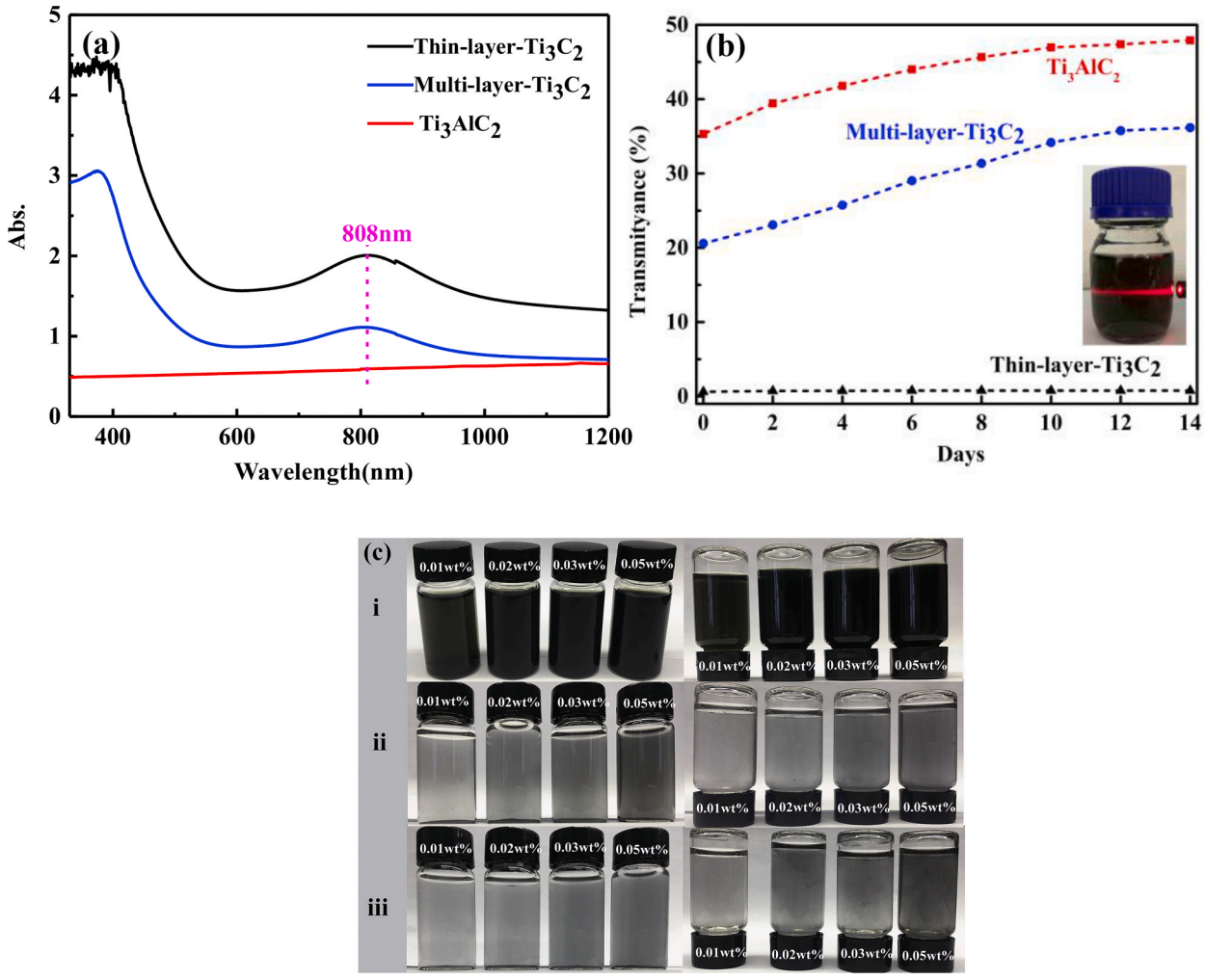

Fig. 4. a) Absorption of Ti_3AlC_2, multi-layer $Ti_3C_2T_x$ and thin-layer $Ti_3C_2T_x$; b)transmittance of nanofluids containing Ti_3AlC_2, multi-layer $Ti_3C_2T_x$ and thin-layer $Ti_3C_2T_x$ with the mass fraction of 0.05 wt% at 808 nm, inset is the Dindal effect of thin-layer $Ti_3C_2T_x$ –H_2O nanofluids; c) photographs of nanofluids with different concentrations: i) thin-layer $Ti_3C_2T_x/H_2O$ nanofluids fresh prepared and stored for 2 weeks, respectively; ii) multi-layer $Ti_3C_2T_x/H_2O$ nanofluids fresh prepared and stored for 2 weeks, respectively; iii) Ti_3AlC_2/H_2O nanofluids fresh prepared and stored for 2 weeks.

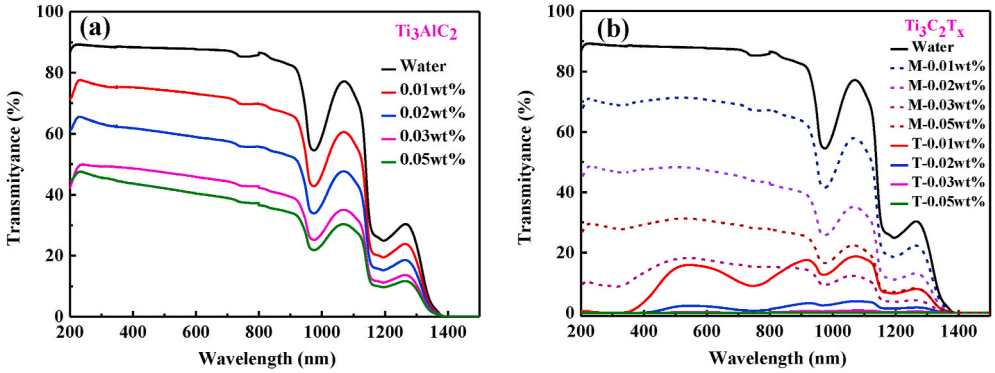

Fig. 5. a) Transmittance spectra of Ti_3AlC_2/H_2O nanofluids with different concentrations; b) transmittance spectra of nanofluids containing multi-layer $Ti_3C_2T_x$ and thin-layer $Ti_3C_2T_x$ with different concentrations (M and T represent multi-layer $Ti_3C_2T_x$ and thin-layer $Ti_3C_2T_x$, respectively).

Ti_3AlC_2 and multi-layer $Ti_3C_2T_x$ are unstable and partial settlement occurs which can also be observed as shown in Fig. 4c–ii and iii, respectively. Unlike Ti_3AlC_2 and multi-layer $Ti_3C_2T_x$, the nanofluids containing thin-layer $Ti_3C_2T_x$ show super colloidal stability and a typical Dindal effect of colloidal as shown in Fig. 4c–i and inset of Fig. 4b. There is no significant change in transmittance even if it has been stored for 14 days (Fig. 4b), which indicates that the nanofluids containing thin-layer $Ti_3C_2T_x$ have excellent stability.

3.2. *Optical properties analysis of $Ti_3C_2T_x$ nanofluids*

The transmittance spectrums of Ti_3AlC_2/H_2O nanofluids and base

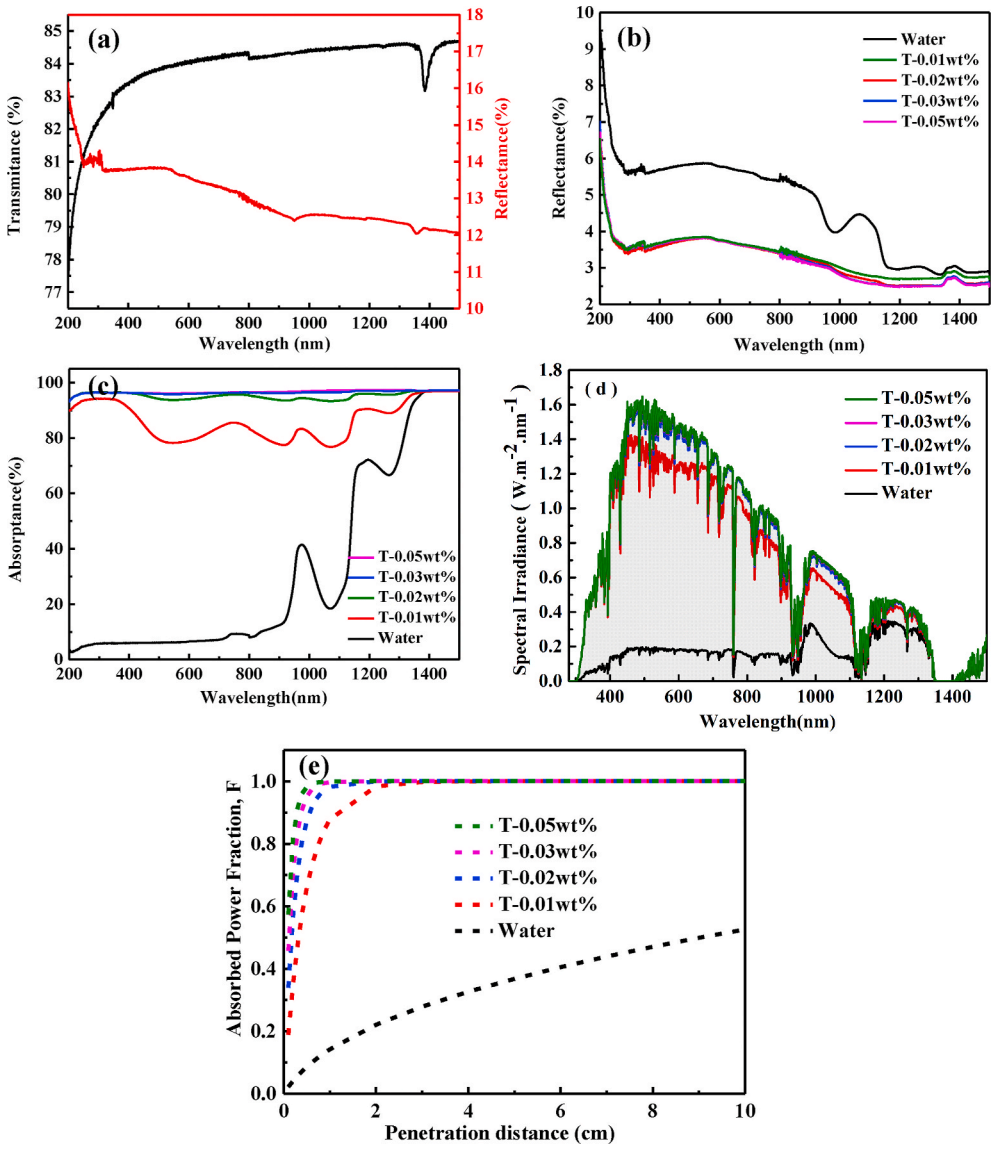

Fig. 6. a) Reflectance and transmittance of the top surface of cuvette; b) reflectance spectra, c) absorptance spectra, d) spectral irradiance and e) absorption power fraction of nanofluids containing thin-layer $Ti_3C_2T_x$ with different concentrations (T represents thin-layer $Ti_3C_2T_x$ and thin-layer $Ti_3C_2T_x$).

fluid are shown in Fig. 5a. As can be seen, with the increase of concentration, the transmittance of nanofluids decreases gradually. It is generally considered that the lower transmittance of fluids, the stronger the optical absorption ability. As it is observed from Fig. 5b, all the nanofluids containing $Ti_3C_2T_x$ exhibit similar behavior to that seen in the Ti_3AlC_2/H_2O nanofluids and show a broadband absorption from 200 to 1500 nm wavelength. It is worthy to point out that the nanofluids containing thin-layer $Ti_3C_2T_x$ show ultra-low transmittance, which is about 40% points lower than that of nanofluids containing multi-layer $Ti_3C_2T_x$ at the same concentration. Hence, the nanofluids containing thin-layer $Ti_3C_2T_x$ may obtain good photo-thermal efficiency.

Fig. 6a shows the transmittance and reflectance of cuvette. It can be seen that the cuvette for sealing nanofluids has high wave transmittance and low strength reflection. Based on the reflectance ($R(\lambda)$) (Fig. 6b) and transmittance ($T(\lambda)$) (Fig. 5b), the absorptance ($\alpha(\lambda)$) (Fig. 6c) of nanofluids containing thin-layer $Ti_3C_2T_x$ with different concentrations can be obtained according to the revised equation:

$$a(\lambda) = 1 - T(\lambda) - R(\lambda) \tag{3}$$

As can be seen from Fig. 6c, the result is consistent with the findings of transmittance spectra (Fig. 5b), with the increase of concentration, the absorptance increases as well. But in high concentration, the effect of concentration becomes weaker. For example, the absorptance increases only from 95.2% to 96.6% when the mass fraction of thin-layer $Ti_3C_2T_x$ is increased from 0.02 wt% to 0.05 wt%. This also gives the reference value to obtain optimal photothermal conversion concentration of nanofluids in the full-spectrum.

The absorbed solar power spectrum of the nanofluid $S_n(\lambda)$ can be expressed as:

$$Sn(\lambda) = a(\lambda)SAM1.5 \tag{4}$$

where $S_{AM1.5}$ is the spectral solar irradiance of AM 1.5 referring to the ASTM G173-03. The spectral irradiance of nanofluids containing thin-layer $Ti_3C_2T_x$ is shown in Fig. 6d. The solar spectral irradiance is indicated by the gray shadow in Fig. 6d. Generally, the absorbed energy can be measured by the area under the curve in the solar spectral irradiance of nanofluids. As can be seen, the spectral irradiance curve of nanofluids is gradually close to the solar spectral irradiance with the increase of concentration. In particular, the curve nearly overlaps with the spectral solar irradiance when the mass fraction of thin-layer $Ti_3C_2T_x$ is 0.03 wt% and 0.05 wt%, indicating that the excellent absorption ability of thin-

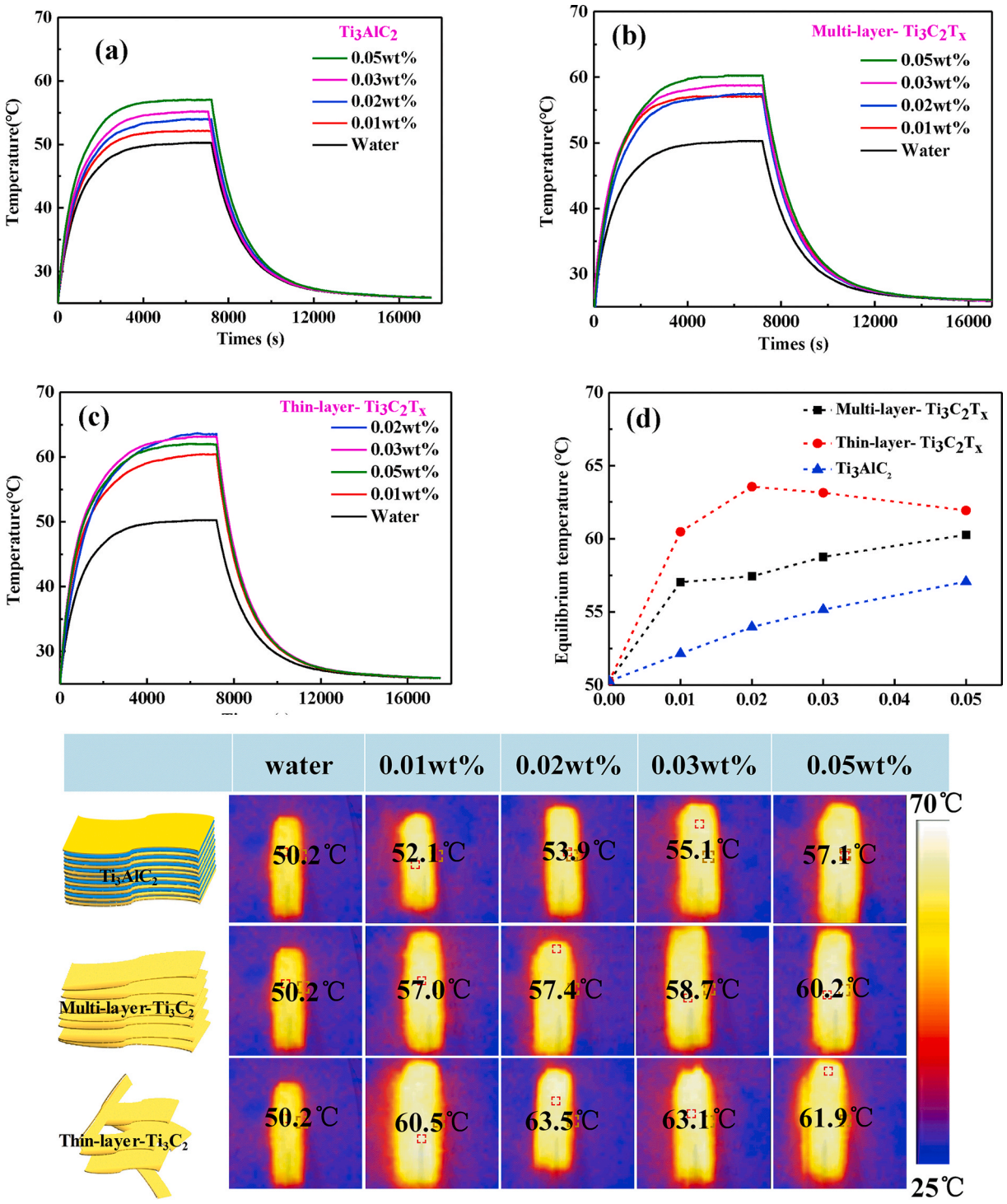

Fig. 7. Temperature rise curves of nanofluids containing a) Ti_3AlC_2, b) multi-layer $Ti_3C_2T_x$ and c) thin-layer $Ti_3C_2T_x$ with different concentrations; d) maximum temperature rise; e) thermal imaging of maximum temperature.

layer $Ti_3C_2T_x$.

The proportion of energy absorbed by nanofluids in the solar spectrum can be expressed by the solar spectrum-weighted stored energy fraction (A_m) which is obtained from equation (4) [37]:

$$Am = \frac{\int_{\lambda min}^{\lambda max} Sn(\lambda)d\lambda}{\int_{\lambda min}^{\lambda max} SAM1.5(\lambda)d\lambda} \quad (5)$$

Fig. 6e shows the A_m of nanofluids containing thin-layer $Ti_3C_2T_x$ with different concentrations. The A_m of all the nanofluids is higher than that of base fluid (DI), suggesting that the absorption capacity could be improved remarkably by adding thin-layer $Ti_3C_2T_x$ into base fluids. It can also be found that the concentration of nanofluids has a great influence on A_m in short penetration distances. However, with the depth of penetration extends, each nanofluids can reach a high value and almost entirely absorb light. This means that the absorption capability can not be improved by increasing the concentration of nanofluids at the long penetration distance. Instead, the absorption efficiency of nanofluids will be weakened owning to the agglomeration of nanoparticles at high concentrations. Additionally, solar radiation is absorbed on the top

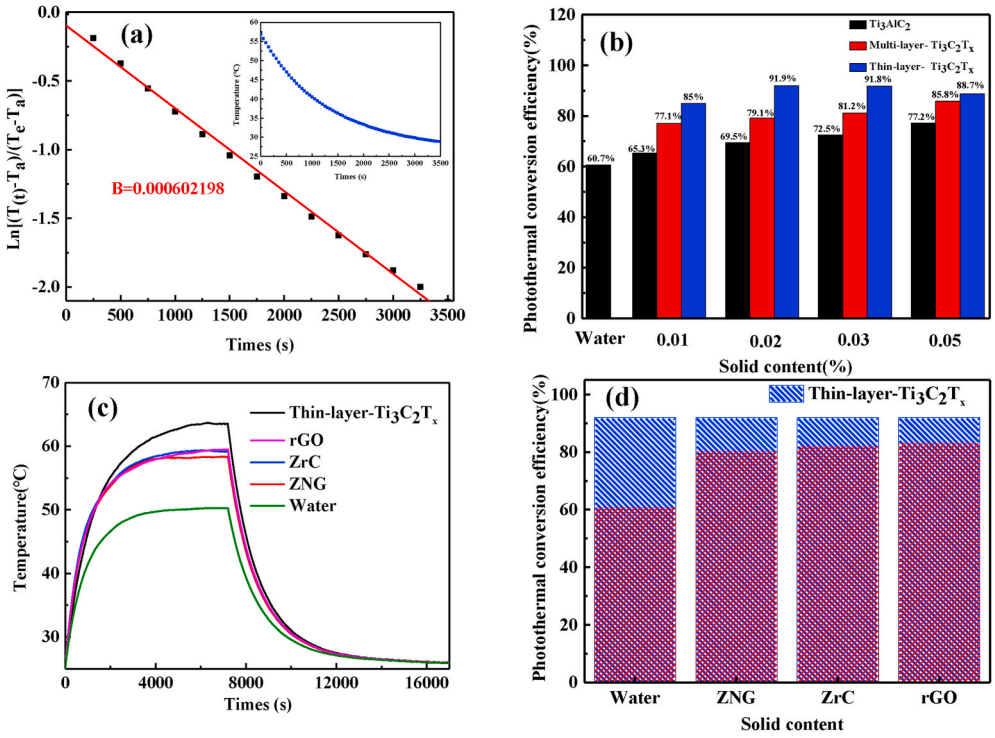

Fig. 8. a)The plotting of $Ln[(t_{(t)}-t_a)/(t_e-t_a)]$ versus time in the cooling stage. Inset is the experimental temperature decay of the nanofluids after switching off the solar simulator; b) photothermal conversion efficiencies of nanofluids; (c) temperature rise and (d) the photothermal conversion efficiencies of nanofluids containing different nanoparticle with the same mass fraction (0.02 wt%).

surface of the nanofluids with high concentration, which is the equivalent of surface absorption, resulting in much heat loss to the environment. Therefore, the concentration of nanofluids must carry on the optimized choice according to the penetration distance. In our work, the depth of receiver is selected as 1.0 cm.

3.3. Photothermal conversion properties of nanofluids

The temperature rise of different nanofluids is shown in Fig. 7a-c. The temperature of all the fluids increases rapidly at the beginning of turning on the solar simulator and as the increase of the irradiation time, the rate becomes slow until an equilibrium status is reached. The main reason for this is that the temperature difference between the liquids and the environment is small, leading to the low heat dissipation rate at the beginning. That is to say, the heat converted by the fluid is much greater than heat dissipation at this moment. However, with the extending of the irradiation time, the temperature of nanofluids increases, and the temperature difference between the liquids and the environment will increase. The heat dissipation began to play their roles, leading to a low temperature rise rate of fluids. Once the thermal equilibrium is achieved, the temperature rise reached a steady state. It is also found that the maximum temperatures of all the nanofluids are higher than that of base fluids (water), suggesting that the photo-thermal conversion efficiency could be improved remarkably by adding nanoparticles into base fluids. As shown in Fig. 7d, the maximum temperatures of nanofluids can be up to 60.5 °C, 63.5 °C, 63.1 °C and 61.9 °C at the mass fraction of thin-layer $Ti_3C_2T_x$ is 0.01 wt%, 0.02 wt%, 0.03 wt% and 0.05 wt%, respectively. The maximum temperatures of nanofluids containing multi-layer $Ti_3C_2T_x$ with the mass fraction of 0.01 wt%, 0.02 wt%, 0.03 wt% and 0.05 wt% reach 57.0 °C, 57.4 °C, 58.7 °C and 60.2 °C, respectively. The maximum temperatures of nanofluids containing Ti_3AlC_2 with the mass fraction of 0.01 wt%, 0.02 wt%, 0.03 wt% and 0.05 wt% reach 52.1 °C, 53.9 °C, 55.1 °C and 57.1 °C, respectively. Significantly, the maximum temperature of nanofluids containing thin-layer $Ti_3C_2T_x$ is higher than that of the other two ones at the same concentration, indicating that thin-layer $Ti_3C_2T_x$ has an excellent photothermal conversion performance.

When the temperature rise curve reaches equilibrium, the solar simulator will be shut down and the cooling process of nanofluids is shown in the inset of Fig. 8a, which can be used to determine the constant rate of heat dissipation (B) by plotting $Ln[(t_{(t)}-t_a)/(t_e-t_a)]$ versus t and fitting the experimental data (Fig. 8a). In this case, $B = 6.02 \times 10^{-4}$. Furthermore, the photothermal conversion efficiency of nanofluids is calculated based on equation (1) as shown in Fig. 8b. It is obvious that the photothermal conversion efficiency tends to be better after the addition of MXene, the photothermal conversion efficiency corresponds with the following order: thin-layer $Ti_3C_2T_x$ > multi-layer $Ti_3C_2T_x$ > water. The maximum photothermal conversion efficiency of nanofluids containing thin-layer $Ti_3C_2T_x$ is up to 91.9%, 31.2% higher than that of water. It can also be seen that the photothermal conversion efficiency of nanofluids containing thin-layer $Ti_3C_2T_x$ decreases with the further increasing concentration of nanofluids, unlike the other two nanofluids. The main reason for this phenomenon is that much solar radiation is absorbed and converted to heat on the top surface of the nanofluids when the thin-layer $Ti_3C_2T_x$ content further increases, which results in much heat loss to the environment.

To further confirm the excellent solar energy absorption property of thin-layer $Ti_3C_2T_x$, some typical nanoparticles including ZNG, ZrC and rGO reported by other researchers [32,34,38] have been tested as a comparison. Fig. 8c shows the temperature rise of nanofluids containing different nanoparticle with the same mass fraction (0.02 wt%). It can be observed that the maximum temperature rise of nanofluids containing thin-layer $Ti_3C_2T_x$ is up to 63.5 °C, which is 4.8 °C, 3.9 °C and 3.7 °C higher than that of ZNG, ZrC and rGO, respectively. Correspondingly, the photothermal conversion efficiency also coincides with the same result (Fig. 8d). All the above experimental results indicate that thin-layer $Ti_3C_2T_x$ is indeed a promising photothermal material.

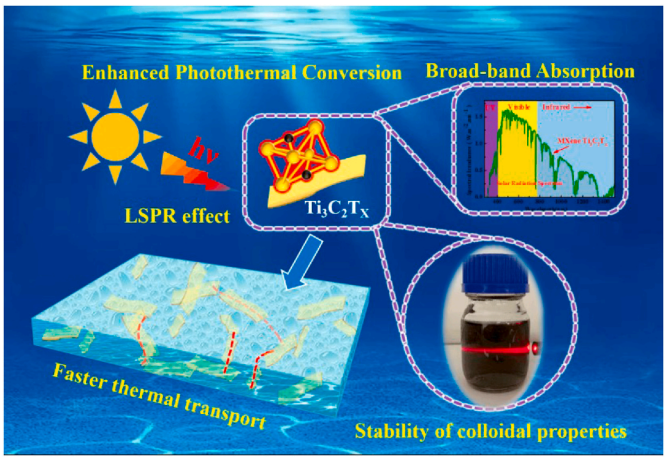

Fig. 9. Radiation energy conversion mechanism of $Ti_3C_2T_x/H_2O$ nanofluids.

3.4. Radiation energy conversion mechanism of $Ti_3C_2T_x$ nanofluids

The light-thermal conversion efficiency of working fluids ($Ti_3C_2T_x/H_2O$ nanofluids) is a key parameter determining the running ability of DASCs. The Radiation energy conversion mechanism of $Ti_3C_2T_x/H_2O$ nanofluids is shown in Fig. 9. Under the irradiation of sunlight, most of the radiation energy is absorbed and converted into heat directly by $Ti_3C_2T_x/H_2O$ nanofluids due to its broadband absorption in 200–1500 nm wavelength. UV–Vis–NIR spectra also shows that the absorption intensity enhances with the increasing concentration of nanofluids. Furthermore, it also exhibits homogeneous thermal behavior and faster thermal transport efficiency in $Ti_3C_2T_x/H_2O$ nanofluids due to its excellent hydrophilicity and high thermal conductivity [39]. But it is worth noting that the photothermal conversion efficiency of nanofluids containing thin-layer $Ti_3C_2T_x$ is higher than that of multi-layer $Ti_3C_2T_x$. Perhaps the main reason is the LSPR effect of $Ti_3C_2T_x$ which can convert the incident light into more heat based on the plasmonic effect.

4. Numerical model of $Ti_3C_2T_x$ nanofluids

4.1. Boundary conditions and model validation

To explain the different light absorption ability of thin-layer $Ti_3C_2T_x$ and multi-layer $Ti_3C_2T_x$, and have a better understanding of the photothermal transformation phenomenon in $Ti_3C_2T_x$ nanofluids, a numerical model is built based on Finite Elements Method (FEM). As shown in Fig. 10a, the incident direction and polarized direction is vertical. In this model, the study domain is wave-frequency domain, and the boundary conditions are set as follows: 1) the $Ti_3C_2T_x$ flake is set as a hexagon with a certain thickness d (18 nm~2 μm) and the radius 2 μm according to the SEM results (Fig. 3b, c); 2) the remaining area is set as pure water to simulate the base fluid system; 3) the whole calculation domain is set as $L_x \times L_y \times L_z = 2.5\mu m \times 2.5\mu m \times 2.5\ \mu m$ and surrounded by perfectly matched layer (PML); 4) all optical parameters of $Ti_3C_2T_x$ are referenced to the results of Alshareef [40]. To examine the reliability of optical parameters used in this work, a comparison has been made between the results by the simulation (Fig. 9b) and that of experiments for absorbance (Fig. 4a), showing good agreement. As Fig. 10b shows, the only difference here is that the absorbance is influenced by the functional groups of the $Ti_3C_2T_x$ leading a new absorbance peak appears around 505 nm which can be ignored [41,42]. Therefore, the parallel incident light wavelength is set as 808 nm in this study.

4.2. Effect of thicknesses of $Ti_3C_2T_x$

Thicknesses are the most obvious difference between multi-layer $Ti_3C_2T_x$ and thin-layer $Ti_3C_2T_x$. To investigate the effect of thicknesses on plasma resonance, the optical field enhancement is introduced which can be measured by $M_{loc} = I_{loc}/I_0$, where $I = 0.5n\varepsilon c_0 E^2$represents optical density, n is the refractive index, ε is the image part of permittivity, therefore the optical field enhancement can be determined from Eq. (5) [43]:

$$M_{loc} = \frac{E_{loc}^{\ 2}}{E_0^{\ 2}} \tag{6}$$

Where E is the amplitude of electrical field which can be calculated from Maxwell equation (6):

$$\nabla \cdot E = \frac{\rho e}{\varepsilon},\ \nabla \cdot H = 0$$

$$\nabla \times E = -\mu \frac{\partial H}{\partial t}$$

$$\nabla \times H = \varepsilon \frac{\partial E}{\partial t} \pm \sigma e E \tag{7}$$

Fig. 11a and Fig. 11b are the thin-layer $Ti_3C_2T_x$ optical field

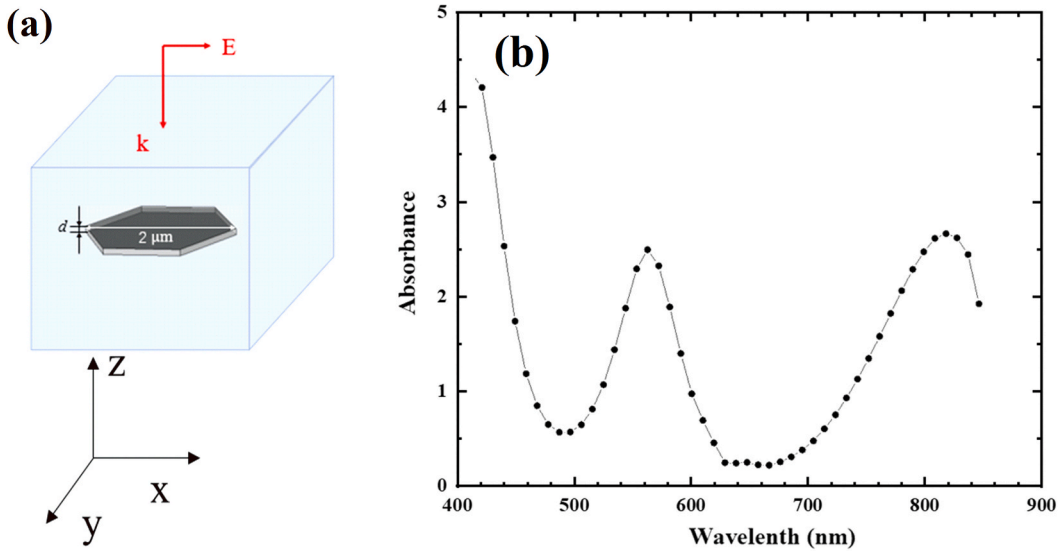

Fig. 10. a) Simulation model structure of $Ti_3C_2T_x$; b) simulation results of absorbance.

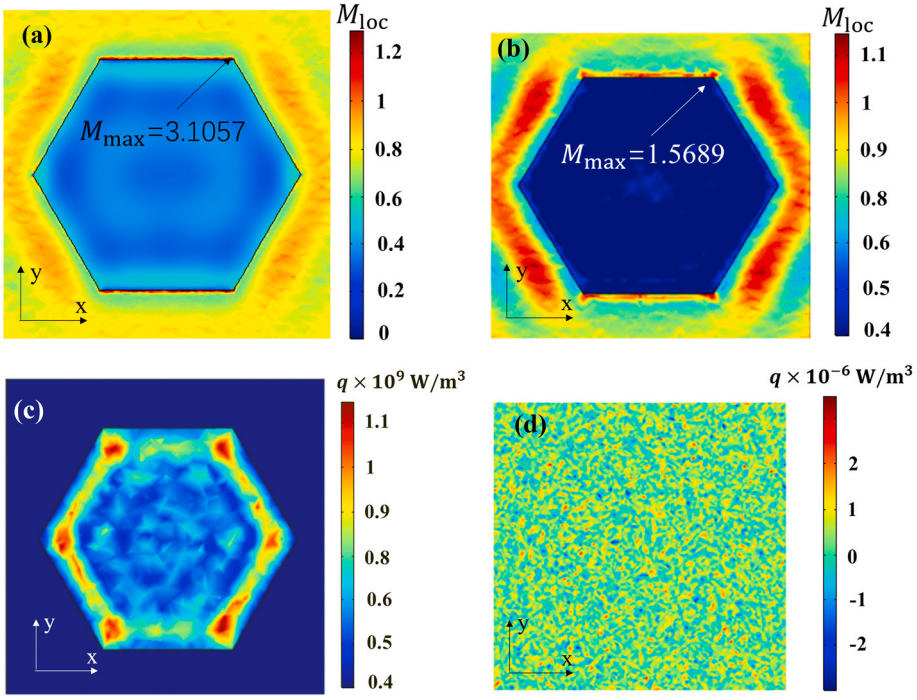

Fig. 11. a) Thin-layer $Ti_3C_2T_x$ optical field enhancement contribution of upper surface (z = 9 nm) when d = 18 nm (~10 layers); b) multi-layer $Ti_3C_2T_x$ optical field enhancement contribution of upper surface (z = 0.5 μm) when d = 1 μm (~555 layers); c) absorbed energy density q of the middle surface ($z = 0$) when $d = 18$ nm. d) absorbed energy density q of model without $Ti_3C_2T_x$ of the middle surface ($z = 0$).

enhancement contribution of the upper surface (z = 9 nm) when d = 18 nm (~10 layers) and multi-layer $Ti_3C_2T_x$ optical field enhancement contribution of the upper surface (z = 0.5 μm) when d = 1 μm (~555 layers), respectively. Compared with the bare fluid model without $Ti_3C_2T_x$ ($M_{loc} \leq 1$), the optical field enhancement of nanofluids containing thin-layer $Ti_3C_2T_x$ and multi-layer $Ti_3C_2T_x$ gets a substantial increase, indicating the strong plasma resonances of $Ti_3C_2T_x$ which also observed by Coppens *et al* [44]. It can be observed from Fig. 11a that the maximum optical field enhancement contribution of upper surface is up to 3.1057 in thin-layer $Ti_3C_2T_x$, which has two times higher enhancement than that of the multi-layer $Ti_3C_2T_x$ ($M_{max} = 1.5689$) (Fig. 11b). That's to say, like other notable metallic nanoparticles such as Au and Ag, $Ti_3C_2T_x$'s LSPR effect is vulnerable to the geometrical parameters of structure [45,46]. Therefore, it is concluded that the extremely high light absorption of $Ti_3C_2T_x/H_2O$ nanofluids is the result of the LSPR effect which can be improved by decreasing thicknesses.

The absorbed energy density q of the middle surface ($z = 0$) in nanofluids containing thin-layer $Ti_3C_2T_x$ ($d = 18$ nm) and bare fluid model without $Ti_3C_2T_x$ are calculated according to the equation $q = 0.5\varepsilon 0\omega \mathrm{Im}(\varepsilon(\omega))E$[47] as shown in Fig. 11c-d. The energy density q is about 10^9 W/m^3 in the $Ti_3C_2T_x$ flake, which is 10^{15} higher than that of the bare fluid model without $Ti_3C_2T_x$. The total energy absorbed Q of fluid is calculated by integrating the fluid domain and material domain as $Q = \iiint qdV$. The energy absorbed by thin-layer $Ti_3C_2T_x/H_2O$ nanofluids is up to 1.3215×10^{-9} W based on the energy integral calculation. Compared with the $Ti_3C_2T_x$ flake's absorption, the water's Radiation energy absorption (6.7525×10^{-27}W) is almost negligible. As for multi-layer $Ti_3C_2T_x$, the absorbed energy (3.1168×10^{-9} W) is only 2.4 times that of thin layer $Ti_3C_2T_x$ even though its volume is 62.5 times that of thin layer. This means that the Radiation energy absorption of the thin-layer flake model is higher than that of multi-layer due to its stronger LSPR effect under the same volume.

4.3. Coupling effect between $Ti_3C_2T_x$ flakes

When the system is irradiated with light, the plasma coupling effect between $Ti_3C_2T_x$ flakes can't be ignored. To investigate the plasma coupling effect on light absorption. Two model structures of thin-layer $Ti_3C_2T_x$ including the undivided model and divided model are designed as shown in Fig. 12a. The distance between their surface is defined as t and 1 $d = 54$ nm $Ti_3C_2T_x$ flake is replaced by 2 $d = 27$ nm to avoid the impact of the added amount of $Ti_3C_2T_x$ in divided model. The optical enhancement distributions of upper surface in undivided model and divided model are shown in Fig. 12b and c, respectively. It can be seen from Fig. 12b that the surrounding optical field of the thin-layer $Ti_3C_2T_x$ has been extremely improved. In the effect of two flakes' plasma coupling, the local optical enhancement is up to 5.0112. In particular, the M_{max} is up to 7.2245 in the sharp corner of the upper flake and the total energy absorbed Q of undivided model is 1.6004×10^{-9} W. By contrast, the maximum optical enhancement of upper surface is only 2.8566 in undivided model as shown in Fig. 12c, which is lower 42.9% than divided model. As a result, the coupling effect improving the light absorption can be triggered by dividing the single flake into two flakes with tiny distance. For further verification of this speculation, the different distances of thin-layer $Ti_3C_2T_x$ are discussed and the results as shown in Fig. 12d. It is found that the energy absorption of thin-layer $Ti_3C_2T_x$ can be significantly improved owing to the LSPR coupling effect.

4.4. Effect of shape of $Ti_3C_2T_x$

Besides all the factors above, the shape of flakes is another important factor that influents the light absorption. To figure it out, the shape of flakes is changed from the hexagon to circle and rectangle under the same volume of thin-layer $Ti_3C_2T_x$ with the thickness $d = 18$ nm as shown in Fig. 13a. The upper surface ($z = 9$ nm) optical enhancement contributions of circle and rectangle are shown in Fig. 13b, c. Although the absorbed energy densities of thin-layer $Ti_3C_2T_x$ with different shapes are all the same (q = 10^9 W/m^3), the Radiation energy absorbed is different due to the different LSPR effect. Compared with $Q = 1.3215 \times 10^{-9}$ in hexagon, the Radiation energy absorbed Q of rectangle model and circle model is 1.3201×10^{-9} W and 1.3057×10^{-9} W, respectively, resulting in 0.1% decrease of rectangle, and 1.2% of circle. This can be

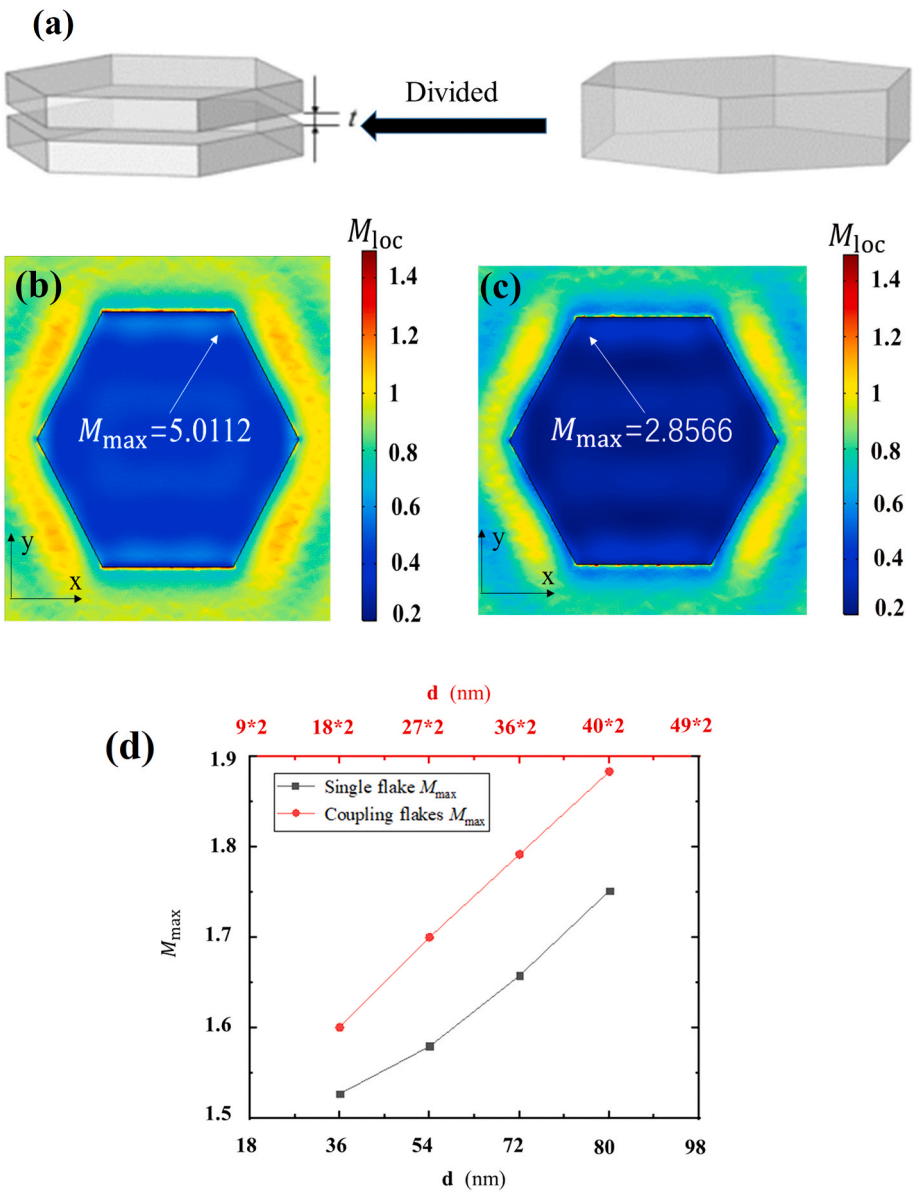

Fig. 12. a) The divided model structure of thin-layer $Ti_3C_2T_x$; b) the optical enhancement distribution of divided model's upper surface when $t = 10$ nm, $d = 27$ nm; c) the optical enhancement distribution of undivided model's upper surface when $d = 54$ nm; d) energy absorption of divided model and undivided model with different layers.

attributed to the plasma resonance of hexagonal thin-layer $Ti_3C_2T_x$ is stronger than other shapes owning to the tip effect in hexagon. In addition, the frequency of rectangular and circular flakes in multi-layer $Ti_3C_2T_x$ is higher than that in thin-layer $Ti_3C_2T_x$, which leads to the higher absorptivity of thin-layer $Ti_3C_2T_x$ than that of multilayer $Ti_3C_2T_x$.

5. Conclusions

Here, we prepare an efficient working fluid ($Ti_3C_2T_x/H_2O$ nanofluids) and investigate its photothermal conversion properties via experiments and numerical simulation. The main conclusions are as follows:

1) $Ti_3C_2T_x/H_2O$ nanofluids show typical Dindal effect of colloidal and super stability, breaking the limitation of fluid instability on direct absorption solar energy collectors (DASCs).
2) The maximum photothermal conversion efficiency is up to 91.9% at a very low mass fraction of 0.02 wt%. The reason for this is that the LSPR effect induced by $Ti_3C_2T_x$ flakes can improve the optical absorption performance of the nanofluids.
3) The influence of nanoscale factors on the optical absorption properties of $Ti_3C_2T_x$ is interpreted by FDTD calculations. Simulation results show that better photothermal performance of thin-layer MXene $Ti_3C_2T_x$ stems from the stronger LSPR effect. Generally, the tiny distance between flakes helps thin-layer $Ti_3C_2T_x$ nanofluids have a stronger LSPR effect than multi-layer. Besides, the shape of $Ti_3C_2T_x$ particles also plays an important role in photothermal absorption and conversion. Due to the tip effect of hexagonal in thin layer $Ti_3C_2T_x$, the light absorbing abilities of thin layer $Ti_3C_2T_x/H_2O$ nanofluids is stronger than multi-layer $Ti_3C_2T_x/H_2O$ nanofluids.

To sum up, this research indicates the $Ti_3C_2T_x/H_2O$ nanofluids' potential in solar energy harvesting.

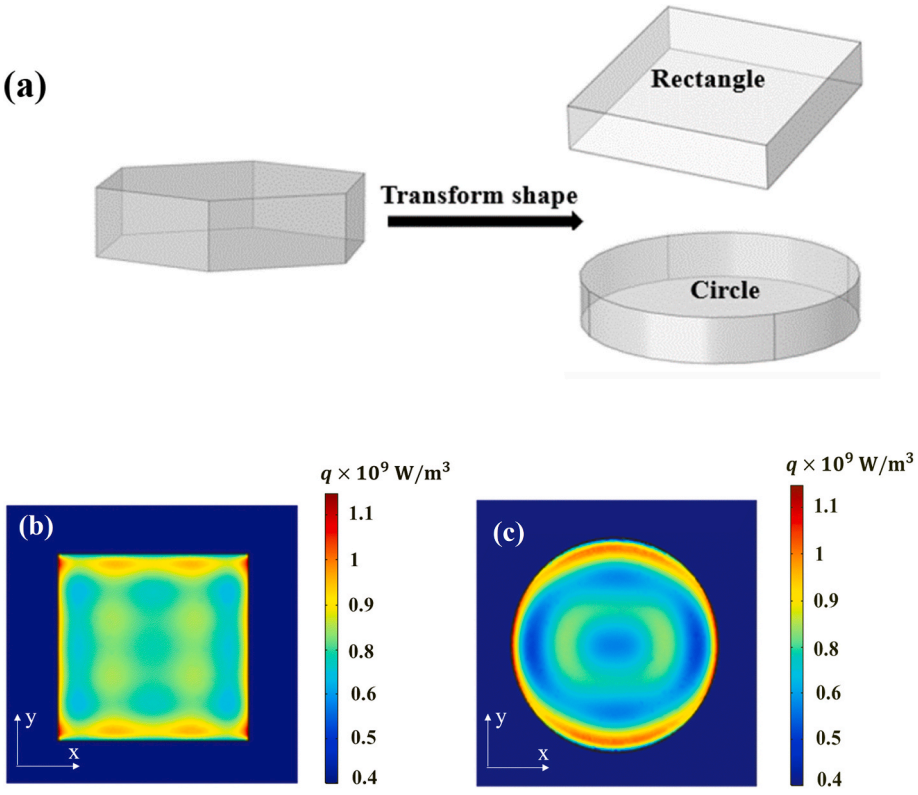

Fig. 13. a) Rectangle and circle model structures after shape changes; b) rectangle thin-layer $Ti_3C_2T_x$ model's optical enhancement of upper surface ($z = 9$ nm); c) circle thin-layer $Ti_3C_2T_x$ model's optical enhancement of upper surface ($z = 9$ nm).

Declaration of competing interest

The authors declare that they have no known competing financial interests or personal relationships that could have appeared to influence the work reported in this paper.

Acknowledgments

The work was supported by National Natural Science Foundation of China (Nos. 51590901, 51576145), the Subject of Shanghai Polytechnic University (Material Science and Engineering; Grant Nos. XXKZD1601), and Gaoyuan Discipline of Shanghai-Environmental Science and Engineering (Resource Recycling Science and Engineering).

References

[1] Y. Zhang, F. Tao, S. Cao, K. Yin, X. Chen, Hierarchical $K_2Mn_4O_8$ nanoflowers: a novel photothermal conversion material for efficient solar vapor generation, Sol. Energ. Mat. Sol. C 200 (2019) 110043, https://doi.org/10.1016/j.solmat.2019.110043.

[2] O. Behar, A novel hybrid solar preheating gas turbine, Energy Convers. Manag. 158 (2018) 120–132, https://doi.org/10.1016/j.enconman.2017.11.043.

[3] J.E. Minardi, H.N. Chuang, Performance of a "black" liquid flat-plate solar collector, Sol. Energy 17 (1975) 179–183, https://doi.org/10.1016/0038-092X(75)90057-2.

[4] O.Z. Sharaf, A.N. Al-Khateeb, D.C. Kyritsis, E. Abu-Nada, Direct absorption solar collector (DASC) modeling and simulation using a novel Eulerian-Lagrangian hybrid approach: optical, thermal, and hydrodynamic interactions, Appl. Energy 231 (2018) 1132–1145, https://doi.org/10.1016/j.apenergy.2018.09.191.

[5] T.B. Gorji, A.A. Ranjbar, A review on optical properties and application of nanofluids in direct absorption solar collectors (DASCs), Renew. Sustain. Energy Rev. 72 (2017) 10–32, https://doi.org/10.1016/j.rser.2017.01.015.

[6] T.P. Otanicar, P.E. Phelan, R.S. Prasher, G. Rosengarten, R.A. Taylor, Nanofluid-based direct absorption solar collector, J. Renew. Sustain. Energy 2 (2010), 033102, https://doi.org/10.1063/1.3429737.

[7] K. Wang, Y. He, A. Kan, W. Yu, D. Wang, L. Zhang, G. Zhu, H. Xie, X. She, Significant photothermal conversion enhancement of nanofluids induced by Rayleigh-Bénard convection for direct absorption solar collectors, Appl. Energy 254 (2019) 113706, https://doi.org/10.1016/j.apenergy.2019.113706.

[8] D. Wang, L. Wang, W. Yu, G. Zhu, J. Zeng, X. Yu, et al., Magnetic photothermal nanofluids with excellent reusability for direct absorption solar collectors, ACS Appl. Energy Mater. 1 (2018) 3860–3868, https://doi.org/10.1021/acsaem.8b0623.

[9] Y. Kameya, K. Hanamura, Enhancement of solar radiation absorption using nanoparticle suspension, Sol. Energy 85 (2011) 299–307, https://doi.org/10.1016/j.solener.2010.11.021.

[10] S.K. Hazra, S. Ghosh, T.K. Nandi, Photo-thermal conversion characteristics of carbon black-ethylene glycol nanofluids for applications in direct absorption solar collectors, Appl. Therm. Eng. 163 (2019) 114402.1–11440213, https://doi.org/10.1016/j.applthermaleng.2019.114402.

[11] M. Maleki, P.T. Ahmadi, H. Mohammadi, H. Karimianb, R. Ahmadic, H.B. M. Emroozc, Photo-thermal conversion structure by infiltration of paraffin in three dimensionally interconnected porous polystyrene-carbon nanotubes (PS-CNT) poly HIPE foam, Sol. Energ. Mat. Sol. C 191 (2019) 266–274, https://doi.org/10.1016/j.solmat.2018.11.022.

[12] J. Tang, X. Jiang, L. Wang, H. Zhang, Z. Hu, Y. Liu, X. Wu, C. Chen, Au@Pt nanostructures: a novel photothermal conversion agent for cancer therapy, Nanoscale 6 (2014) 3670–3678, https://doi.org/10.1039/c3nr06841b.

[13] S. Zhou, L. Shang, Y. Zhao, R. Shi, G.I.N. Waterhouse, Y. Huang, L. Zheng, T. Zhang, Pd single-atom catalysts on nitrogen-doped graphene for the highly selective photothermal hydrogenation of acetylene to ethylene, Adv. Mater. 31 (2019) 1900509, https://doi.org/10.1002/adma.201900509.

[14] M. Belekoukia, E. Kalamaras, J.Z.Y. Tan, F. Vilela, S. Garcia, M.M. Maroto-Valer, J. Xuan, Continuous flow-based laser-assisted plasmonic heating: a new approach for photothermal energy conversion and utilization, Appl. Energy 247 (2019) 517–524, https://doi.org/10.1016/j.apenergy.2019.04.069.

[15] M. Noroozi, B. Mohammadi, S. Radiman, Z. Azmi, R.S. Azis, Photothermal effect of modulating laser irradiation on the thermal diffusivity of Al_2O_3 Nanofluids, Nanoscale Res. Lett. 14 (2019) 1–10, https://doi.org/10.1186/s11671-019-2869-2.

[16] L. Huang, N. Yi, Y. Wu, Y. Zhang, Q. Zhang, Y. Huang, Y. Ma, Y. Chen, Multichannel and repeatable self-healing of mechanical enhanced graphene-thermoplastic polyurethane composites, Adv. Mater. 25 (2013) 2224–2228, https://doi.org/10.1002/adma.201204768.

[17] Z. Xiang, L. Zhang, Y. Li, T. Yuan, W. Zhang, J. Sun, Reduced graphene oxide reinforced polymeric films with excellent mechanical robustness and rapid and highly efficient healing properties, ACS Nano 11 (2017) 7134–7141, https://doi.org/10.1021/acsnano.7b02970.

[18] A.R. Mallah, M.N. Zubir, O.A. Alawi, K.M. Newaz, A.B. Badry, Plasmonic nanofluids for high photothermal conversion efficiency in direct absorption solar collectors: fundamentals and applications, Sol. Energ. Mat. Sol. C 201 (2019) 110084, https://doi.org/10.1016/j.solmat.2019.110084.

[19] S.C. Warren, E. Thimsen, Plasmonic solar water splitting, Energy Environ. Sci. (5) (2012) 5133–5146, https://doi.org/10.1039/C1EE02875H.
[20] P. Pallavicini, A.D.A. Taglietti, P. Minzioni, M. Patrini, G. Dacarro, G. Chirico, L. Sironi, N. Bloise, L. Visai, L. Scarabelli, Self-assembled monolayers of gold nanostars: a convenient tool for near-IR photothermal biofilm eradication, Chem. Commun. 50 (2014) 1969–1971, https://doi.org/10.1039/c3cc48667b.
[21] L. Wang, G. Zhu, W. Yu, D. Zhu, Y. Zhang, L. Zhang, H. Xie, Y. Zhang, L. Zhang, H. Xie, Photothermal properties of near-spherical gold nanofluids with strong localized surface plasmon resonance, J. Therm. Sci. Eng. Appl. 10 (2018) 5, https://doi.org/10.1115/1.4036800, 011015.
[22] A.S. Abdelrazik, K.H. Tan, N. Aslfattahi, A. Arifutzzaman, R. Saidur, F.A. Al-Sulaiman, Optical, stability and energy performance of water-based MXene nanofluids in hybrid PV/thermal solar systems, Sol. Energy 204 (2020) 32–47, https://doi.org/10.1016/j.solener.2020.04.063.
[23] L. Das, K. Habib, R. Saidur, N. Aslfattahi, S. M. Yahya, F. Rubbi, Improved thermophysical properties and energy efficiency of qqueous Ionic liquid/MXene nanofluid in a hybrid PV/T solar system, Nanomaterials, 10 (7), https://doi.org/10.3390/nano10071372.
[24] M.S. Cao, Y.Z. Cai, P. He, J. Shu, W. Cao, J. Yuan, 2D MXenes: electromagnetic property for microwave absorption and electromagnetic interference shielding, Chem. Eng. J. 359 (2019) 1265–1302, https://doi.org/10.1016/j.cej.2018.11.051.
[25] Y. Wen, T.E. Rufford, X. Chen, N. Li, M. Lyu, L. Dai, L. Wang, Nitrogen-doped $Ti_3C_2T_x$ MXene electrodes for high-performance supercapacitors, Nanomater. Energy 38 (2017) 368–376, https://doi.org/10.1016/j.nanoen.2017.06.009.
[26] Y. Krishna, M. Faizal, R. Saidur, K.C. Ng, N. Aslfattahi, State-of-the-art heat transfer fluids for parabolic trough collector, Int. J. Heat Mass Tran. 152 (2020) 119541, https://doi.org/10.1016/j.ijheatmasstransfer.2020.119541.
[27] F. Shahzad, M. Alhabeb, C.B. Hatter, B. Anasori, H.S. Man, C.M. Koo, Y. Gogotsi, Electromagnetic interference shielding with 2D transition metal carbides (MXenes), Science 353 (2016) 1137–1140, https://doi.org/10.1126/science.aag2421.
[28] H. Lin, X. Wang, L. Yu, Y. Chen, J. Shi, Two-dimensional ultrathin Mxene ceramic nanosheets for photothermal conversion, Nano Lett. 17 (2017) 384–391, https://doi.org/10.1021/acs.nanolett.6b04339.
[29] N. Parashar, N. Aslfattahi, S.M. Yahya, R. Saidur, An artificial neural network approach for the prediction of dynamic viscosity of MXene-palm oil nanofluid using experimental data, J. Therm. Anal. Calorim. (2020), https://doi.org/10.1007/s10973-020-09638-3.
[30] R. Li, L. Zhang, L. Shi, P. Wang, MXene Ti_3C_2: an effective 2D light-to-heat conversion material, ACS Nano 11 (2017) 3752–3759, https://doi.org/10.1021/acsnano.6b08415.
[31] N. Aslfattahi, L. Samylingam, A.S. Abdelrazik, A. Arifutzzaman, R. Saidur, MXene based new class of silicone oil nanofluids for the performance improvement of concentrated photovoltaic thermal collector, Sol. Energ. Mat. Sol. C 211 (2020) 110526, https://doi.org/10.1016/j.solmat.2020.110526.
[32] L. Wang, G. Zhu, W. Yu, J. Zeng, X. Yu, Q. Li, H. Xie, Integrating nitrogen-doped graphitic carbon with Au nanoparticles for excellent solar energy absorption properties, Sol. Energ. Mat. Sol. C 184 (2018) 1–8, https://doi.org/10.1016/j.solmat.2018.04.028.
[33] L. Wang, G. Zhu, M. Wang, W. Yu, J. Zeng, X. Yu, Q. Li, H. Xie, Dual plasmonic Au/TiN nanofluids for efficient solar photothermal conversion, Sol. Energy 184 (2019) 240–248, https://doi.org/10.1016/j.solener.2019.04.013.
[34] Z. Meng, Y. Li, N. Chen, D. Wu, H. Zhu, Broad-band absorption and photo-thermal conversion properties of zirconium carbide aqueous nanofluids, J. Taiwan Inst. Chem. E 80 (2017) 286–292, https://doi.org/10.1016/j.jtice.2017.07.010.
[35] R.J. Moffat, Using uncertainty analysis in the planning of an experiment, J. Fluid Eng. 107 (1985) 173–178, https://doi.org/10.1115/1.3242452.
[36] X. Fan, Y. Ding, Y. Liu, J. Liang, Y. Chen, Plasmonic $Ti_3C_2T_x$ Mxene enables highly efficient photothermal conversion for healable and transparent wearable device, ACS Nano 13 (2019) 8124–8134, https://doi.org/10.1021/acsnano.9b03161.
[37] W.D. Drotning, Optical properties of solar-absorbing oxide particles suspended in a molten salt heat transfer fluid, Sol. Energy 20 (1978) 313–319, https://doi.org/10.1016/0038-092X(78)90123-8.
[38] D. Wang, Y. Jia, Y. He, L. Wang, H. Xie, W. Yu, Photothermal efficiency enhancement of a nanofluid-based direct absorption solar collector utilizing magnetic nano-rotor, Energy Convers. Manag. 199 (2019) 111996, https://doi.org/10.1016/j.enconman.2019.111996.
[39] R. Liu, W. Li, High-thermal-stability and high-thermal-conductivity $Ti_3C_2T_x$ MXene/Poly (vinyl alcohol) (PVA) Composites, ACS Omega 3 (2018) 2609–2617, https://doi.org/10.1021/acsomega.7b02001.
[40] K. Ehad, S.L. El-Demellawi, J. Yin, O.F. Mohammed, H.N. Alshareef, Tunable multipolar surface plasmons in 2D $Ti_3C_2T_x$ MXene flakes, ACS Nano 12 (2018) 8485–8493, https://doi.org/10.1021/acsnano.8b04029.
[41] X. Sheng, Y. Zhao, L. Zhang, X. Lu, Properties of two-dimensional Ti_3C_2 MXene/thermoplastic polyurethane nanocomposites with effective reinforcement via melt blending, Compos. Sci. Technol. 181 (2019) 107710, https://doi.org/10.1016/j.compscitech.2019.107710.
[42] M. Hu, T. Hu, Z. Li, Y. Yang, R. Cheng, J. Yang, C. Cui, X. Wang, Surface functional groups and interlayer water determine the electrochemical capacitance of $Ti_3C_2T_x$ MXene, ACS Nano 12 (2018) 3578–3586, https://doi.org/10.1021/acsnano.8b00676.
[43] Y. Chen, Y. Xu, D. Xie, J. Jiang, Y. Yue, Simulation on tip-assisted focusing of laser energy for sub-surface photon heating, Appl. Therm. Eng. 148 (2019) 129–135, https://doi.org/10.1016/j.applthermaleng.2018.11.050.
[44] Z.J. Coppens, W. Li, D.G. Walker, J.G. Valentine, Probing and controlling photothermal heat generation in plasmonic nanostructures, Nano Lett. 13 (2013) 1023–1028, https://doi.org/10.1021/nl304208s.
[45] Y. Qi, T. Xing, J. Zhao, G. Weng, Jian-jun Li, Jian Zhu, Jun-wu Zhao, Tuning the surface enhanced Raman scattering performance of anisotropic Au core-Ag shell hetero-nanostructure: the effect of core geometry, J. Alloys Compd. 776 (2019) 934–947, https://doi.org/10.1016/j.jallcom.2018.10.321.
[46] H. George, J. Chan, E.M. Hicks, G.C. Schatz, R.P.V. Duyne, Plasmonic properties of copper nanoparticles fabricated by nanosphere lithography, Nano Lett. 7 (2007) 1947–1952, https://doi.org/10.1021/nl070648a.
[47] Y. Cai, J. Zhu, Q. Liu, Tunable enhanced optical absorption of graphene using plasmonic perfect absorbers, Appl. Phys. Lett. 106 (2015), 043105, https://doi.org/10.1063/1.4906996.